Journal of Materials Chemistry C

PAPER

View Article Online
View Journal | View Issue

Cite this: J. Mater. Chem. C, 2017, 5, 208

Homoleptic thiazole-based Ir^{III} phosphorescent complexes for achieving both high EL efficiencies and an optimized trade-off among the key parameters of solution-processed WOLEDs†

Haoran Guo,[a] Jiang Zhao,[a] Zhuanzhuan Tian,[a] Yong Wu,[a] Boao Liu,[a] Feifan Dang,[a] Xiaolong Yang,[a] Guijiang Zhou,*[a] Zhaoxin Wu*[b] and Wai-Yeung Wong*[cd]

Received 14th September 2016,
Accepted 20th November 2016

DOI: 10.1039/c6tc04011j

www.rsc.org/MaterialsC

Two homoleptic thiazole-based Ir^{III} phosphorescent emitters, **Ir-3Tz1F** and **Ir-3Tz2F**, with fluorinated 2-phenylthiazole-type ligands were designed and prepared. Their thermal stability, and photophysical and electrochemical properties, as well as electroluminescent (EL) performances in both monochromic OLEDs and solution-processed WOLEDs were investigated. When doped in monochromic OLEDs made by vacuum deposition, **Ir-3Tz1F** gave the maximum EL efficiencies with η_L of 56.2 cd A^{-1}, η_{ext} of 15.8% and η_p of 50.2 lm W^{-1}. Critically, solution-processed WOLEDs based on **Ir-3Tz1F** with three primary colors could achieve an excellent trade-off among the stable balanced white EL spectra, a high EL efficiency and a high color rendering index (CRI). The optimized solution-processed WOLED exhibited very attractive EL efficiencies of 33.4 cd A^{-1}, 16.5% and 30.6 lm W^{-1}, while maintaining both a high CRI of *ca.* 80 and very stable Commission Internationale de L'Eclairage (CIE) coordinates in a wide driving voltage range from 4 V to 11 V.

Introduction

Regarded as a hybrid of an electron-deficient pyridyl moiety and an electron-rich thiophenyl ring,[1] the thiazolyl group can afford distinct electronic features to tune the photophysical properties of phosphorescent Ir^{III}/Pt^{II} 2-phenylpyridine (ppy)-type complexes bearing thiazole-based ligands, since the emission color, the phosphorescent quantum yield (Φ_P), the phosphorescent lifetime (τ_P) and the charge carrier injection/transporting properties of these phosphorescent (triplet) complexes can be greatly affected by the electronic structures of the chelated organic ligands.[2–10] All of these photophysical properties can play a critical role in optimizing the electroluminescent (EL) performances of the concerned phosphorescent (triplet) complexes in organic light-emitting diodes (OLEDs), which then show great potential in the development of both new-generation flat panel displays and future energy-saving lighting sources.[11–15] More commonly, it is the benzothiazole rather than thiazole group that has been employed to construct the ligands of phosphorescent Ir^{III}/Pt^{II} ppy-type complexes.[3,16] Quite a number of benzothiazole-based Ir^{III} ppy-type triplet emitters have been developed that show high EL efficiencies.[17–22] Furthermore, some functional groups, such as carbazole,[21] dibenzothiophene-*S*,*S*-dioxide[18] and the triphenylphosphoryl unit,[18] have been introduced to furnish carrier injection/transporting capabilities to the concerned benzothiazole-based Ir^{III} ppy-type triplet emitters to optimize their EL performances.

Recently, the thiazole group has been introduced to ppy-type ligands to develop thiazole-based phosphorescent Ir^{III}/Pt^{II} emitters.[23–26] We have prepared ppy-type triplet emitters with either 2-naphthylthiazole-type[23] or 2-phenylthiazole-type[25] ligands. It was shown that the phosphorescence color of the complexes can be tuned by the substitution position of the thiazole unit on the naphthalene[23] and the fluorine group attached to the ligands.[25] Furthermore, the substitution position of the thiazole unit can also exert a great influence on the EL efficiencies of the naphthylthiazole-type phosphorescent Ir^{III}/Pt^{II} emitters.[23]

[a] MOE Key Laboratory for Nonequilibrium Synthesis and Modulation of Condensed Matter, Institute of Chemistry for New Energy Material, Department of Chemistry, School of Science, State Key Laboratory for Mechanical Behavior of Materials, Xi'an Jiaotong University, Xi'an 710049, P. R. China. E-mail: zhougj@mail.xjtu.edu.cn; Fax: +86-29-8266-3914
[b] Key Laboratory for Physical Electronics and Devices of the Ministry of Education, Faculty of Electronic and Information Engineering, Xi'an Jiaotong University, Xi'an 710049, P. R. China. E-mail: zhaoxinwu@mail.xjtu.edu.cn
[c] Institute of Molecular Functional Materials and Department of Chemistry, Hong Kong Baptist University, Waterloo Road, Kowloon Tong, Hong Kong, P. R. China. E-mail: rwywong@hkbu.edu.hk
[d] Department of Applied Biology and Chemical Technology, The Hong Kong Polytechnic University, Hung Hom, Hong Kong, P. R. China. E-mail: wai-yeung.wong@polyu.edu.hk

† Electronic supplementary information (ESI) available: EL data including EL spectra, *J*–*V*–*L* and EL efficiency curves. See DOI: 10.1039/c6tc04011j

In addition, the functional groups, such as triphenylamine (TPA)[24] and carbazole,[26] have also been combined with thiazole to prepare novel thiazole-based ligands, which have been chelated with an Ir^{III} center to develop functionalized phosphorescent emitters with attractive EL performances. All of these results indicate a great potential for thiazole-based phosphorescent emitters in the field of OLEDs. Unfortunately, they are relatively rare and generally have a heteroleptic configuration.

Due to the inherent electronic features associated with the thiazole unit, thiazole-based phosphorescent Ir^{III} emitters typically exhibit a bathochromic effect in the phosphorescent wavelength with respect to that of their pyridine-based analogues.[24,26] Therefore, they generally emit orange/yellow phosphorescence, which can be coupled with blue emission to construct white organic light-emitting diodes (WOLEDs) of complementary colors.[24] Thiazole-based phosphorescent Ir^{III} emitters bearing a TPA functional group have been applied to complementary colored WOLEDs, which have shown decent EL efficiencies.[24] However, the white EL spectra for the concerned WOLEDs vary markedly under different driving voltages, leading to a great variation in both the Commission Internationale de L'Eclairage (CIE) coordinates and the color rendering index (CRI).[24] Some WOLEDs with a single emission layer also show voltage-dependent white EL spectra.[27,28] In addition, there is a trade-off issue between the luminous efficiency and the color quality for white emission from WOLEDs. This means that the trichromatic WOLEDs with red, green and blue (R–G–B) emitters typically have a better color quality, but lower EL efficiency.[15] All these issues are really undesirable for the practical application of WOLEDs as new energy-saving lighting sources. Therefore it is necessary to develop new thiazole-based phosphorescent emitters with diverse properties and structures to cope with the critical problems in the field of OLEDs, particularly those associated with WOLEDs. Therefore, in the present study, two homoleptic phosphorescent thiazole-based ppy-type Ir^{III} emitters were developed to furnish not only high efficiency monochromic OLEDs, but also address the optimized trade-off in solution-processed WOLEDs with a single doped emission layer.

Experimental

Spectroscopy

UV/Vis spectra were recorded with a Shimadzu UV-2250 spectrophotometer. The steady-state photoluminescent (PL) properties of the complexes were measured with Edinburgh FLS920 fluorometers. The phosphorescence quantum yields (Φ_P) were determined in degassed CH_2Cl_2 solution at 298 K against the *fac*-[$Ir(ppy)_3$] standard (Φ_P = 0.40).[29] The lifetimes were measured with a single photon counting spectrometer from Edinburgh Instruments (FLS-920) with a picosecond pulse LED excitation source. The data analysis was conducted by iterative convolution of the luminescence decay profile with the instrument response function using the software package provided by Edinburgh Instruments. DSC was performed with a NETZSCH DSC 200 PC unit under a nitrogen flow at a heating rate of 10 °C min^{-1}. TGA was conducted with a NETZSCH STA 409C instrument under nitrogen with a heating rate of 20 °C min^{-1}. Fast atom bombardment (FAB) mass spectra were recorded with a Finnigan MAT SSQ710 system. ^1H, ^{13}C and ^{19}F NMR spectra were recorded on a Bruker Avance 400 MHz spectrometer.

Cyclic voltammetry studies

Electrochemical measurements were performed using a Princeton Applied Research 2273A potentiostat. Cyclic voltammetry (CV) of the sample solutions was performed at a scan rate of 100 mV s^{-1} using a glassy carbon working electrode, a platinum counter electrode, and a platinum-wire reference electrode. The solvent was deoxygenated acetonitrile, and the supporting electrolyte was 0.1 M [$n$$Bu_4N$][$BF_4$]. Ferrocene (Fc) was added as a calibrant after each set of measurements, and all the potentials reported are quoted with reference to the ferrocene/ferrocenium (Fc/Fc^+) couple. The HOMO energy level was obtained using the following equation: $E_{HOMO} = -(E_a + 4.8)$ eV.[30] However, the LUMO energy level was determined from $E_{LUMO} = (E_g + E_{HOMO})$ eV (E_g: optical band gap derived from the absorption onset in the UV/Vis spectra).

Synthesis

All the reactions were conducted under a nitrogen atmosphere and no special precautions were required during workup. The solvents were carefully dried and distilled from appropriate drying agents prior to use. Commercially available reagents were used without further purification unless otherwise stated. All the reactions were monitored by TLC with Merck pre-coated aluminum plates. Flash column chromatography was carried out using silica gel (200–300 mesh). [$Ir(acac)_3$], organic boric acid and 2-bromothiazole were purchased from Sigma-Aldrich. The organic ligands **L1** and **L2** were prepared following our published strategy.[25] The red phosphorescent emitter **Ir-G1** was obtained from our laboratory and the details of its preparation were provided in our previous report.[31]

Typical procedure for synthesizing the complexes Ir-3Tz1F and Ir-3Tz2F

Under an N_2 atmosphere, the corresponding organic ligand (3.5 equiv.) and [$Ir(acac)_3$] (1.0 equiv.) were added to glycerol. The resulting mixture was stirred at *ca.* 220 °C for 10 h. After completion of the reaction, 1.0 M aqueous hydrochloric acid was added to the solution, resulting in precipitation of the colored crude product, which was filtered, washed with water and dried at 100 °C under vacuum. The purification of the product was carried out using silica-gel column chromatography eluting with CH_2Cl_2/hexane (2 : 1, v/v). The concerned complex was obtained as a yellow solid.

Ir-3Tz1F. Yield: 31%. ^1H NMR (400 MHz, $CDCl_3$): δ (ppm) 7.50 (dd, J = 8.4 Hz, 5.6 Hz, 3H, Ar), 7.11 (d, J = 3.2 Hz, 3H, Ar), 6.80 (d, J = 3.6 Hz, 3H, Ar), 6.62–6.57 (m, 3H, Ar), 6.48 (d, J = 2.4 Hz, 3H, Ar). ^{13}C NMR (100 MHz, $CDCl_3$): δ (ppm) 177.20, 165.33, 162.81, 159.45, 159.39, 139.48, 136.74, 126.03, 125.93, 122.80, 122.63, 116.61, 107.98, 107.74. ^{19}F NMR (376 MHz, $CDCl_3$): δ (ppm) −110.36 (s, 3F). FAB-MS: m/z = 727 $[M]^+$.

$C_{27}H_{15}F_3IrN_3S_3$: calcd C 44.62, H 2.08, N 5.78; found C 44.48, H 2.12, N 5.69.

Ir-3Tz2F. Yield: 27%. ^{1}H NMR (400 MHz, $CDCl_3$): δ (ppm) 7.30 (dd, J = 3.2 Hz, 3H, Ar), 6.89 (t, J = 1.6 Hz, 3H, Ar), 6.46 (dd, J = 8.8 Hz, 17.2 Hz, 3H, Ar), 6.38 (dd, J = 2 Hz, 9.2 Hz, 3H, Ar). ^{13}C NMR (100 MHz, $CDCl_3$): δ (ppm) 176.16, 164.71, 159.93, 159.87, 139.87, 137.75, 126.92, 126.82, 121.75, 121.59, 120.25, 108.09, 107.85. ^{19}F NMR (376 MHz, $CDCl_3$): δ (ppm) −106.50 (d, 1F), −108.91 (d, 1F). FAB-MS: m/z = 781 $[M]^+$. $C_{27}H_{12}F_6IrN_3S_3$: calcd C 41.53, H 1.55, N 5.38; found C 41.37, H 1.39, N 5.27.

OLED fabrication and measurements

The pre-cleaned ITO glass substrates were treated with ozone for 20 min. A thin MoO_3 layer was deposited on the surface of the ITO glass to form a 4 nm-thick hole-injection layer. Then, a 50 nm-thick layer of **CBP** with a 15 nm local doping zone was constructed to serve as both the hole-transporting and emission layers. After that, **TPBi** (40 nm), LiF (1 nm) and the Al cathode (100 nm) were successively evaporated. For the fabrication of the WOLEDs, PEDOT:PSS was first deposited on the treated ITO glass by applying a spin-coating strategy. Then, the ITO-coated glass was dried at *ca.* 100 °C for 1 h. The chloroform solution containing the host materials and emitters was spin-coated with a concentration of *ca.* 10 mg mL^{-1}. After drying at *ca.* 50 °C for 0.5 h, other functional layers of **TPBi** (40 nm), LiF (1 nm) and the Al cathode (100 nm) were successively evaporated. All the evaporation processes were conducted at a base pressure of less than 10^{-6} Torr. The EL spectra and CIE coordinates were measured with a PR650 spectra colorimeter. The *J–V–L* curves of the devices were recorded by a Keithley 2400/2000 source meter and the luminance was measured using a PR650 SpectraScan spectrometer. All the experiments and measurements were carried out under ambient conditions.

Computational details

Density functional theory (DFT) calculations using the B3LYP functional were performed for all the Ir^{III} complexes and their geometries were obtained by theoretical optimization during the computation. The basis set used for the C, H, F, N and O atoms was 6-31G, whereas effective core potentials with a LanL2DZ basis set were employed for the S and Ir atoms.[32,33] The energies of the excited states of the complexes were computed by time-dependent (TD) DFT (TD-DFT) based on all the ground-state geometries. All the calculations were carried out using the Gaussian 09 program.[34] Mulliken population analyses were performed using MullPop.[35] Frontier molecular orbitals obtained from the DFT calculations were plotted using the Molden 3.7 program.[36]

Results and discussion

Synthesis and characterization

The synthetic procedure for the thiazole-based homoleptic Ir^{III} ppy-type phosphorescent emitters is shown in Scheme 1. In order to prepare the complexes, the organic ligands **L1** and **L2** should be synthesized first *via* a Suzuki cross-coupling reaction between 2-bromothiazole and the corresponding fluorinated phenyl boronic acid with $Pd(PPh_3)_4$ as the catalyst. With the aim to tune the maximum phosphorescent wavelength of the complexes, a fluorine substituent was introduced to the organic ligands. All the ligands could be easily obtained in good yields over 80%. After obtaining the organic ligands, the two homoleptic phosphorescent Ir^{III} complexes were prepared according to the well-established one-pot strategy by the cyclometalation of $[Ir(acac)_3]$ (acac: acetylacetone anion) with the corresponding organic ligands in glycerol at *ca.* 220 °C.[4,23,24] The homoleptic Ir^{III} complexes were purified by silica-gel chromatography in high purity as air-stable yellow powders.

In the ^{1}H NMR spectra of the two homoleptic Ir^{III} complexes, only one set of signals assigned to the protons of the three thiazole-based ligands, corresponding to the *fac*-isomers, were obtained for both **Ir-3Tz1F** and **Ir-3Tz2F**. In the ^{19}F NMR spectrum of **Ir-3Tz1F**, the single resonance peak at *ca.* −110.36 ppm indicates the only –F group on the chelated phenyl ring of the thiazole-based ligand. For **Ir-3Tz2F**, the two sets of double resonance peaks at *ca.* −106.50 ppm and −108.91 ppm in its

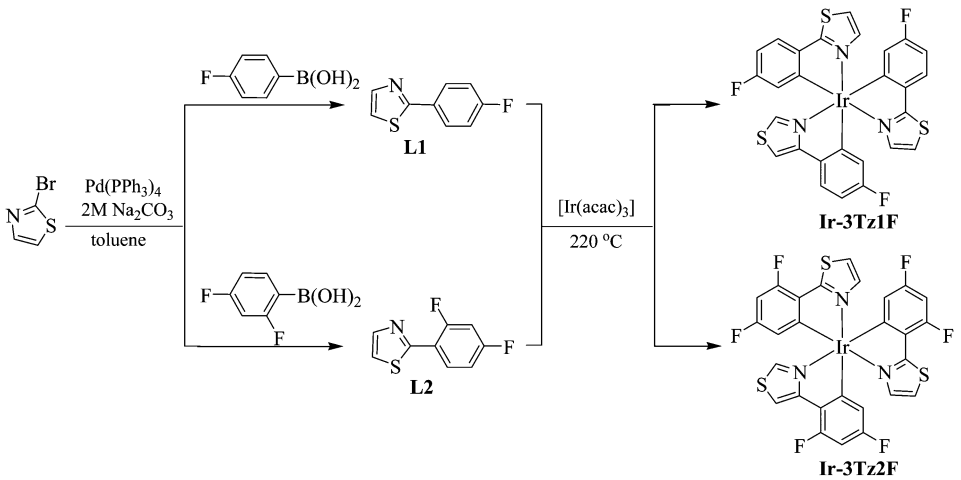

Scheme 1 Synthetic sketches for the thiazole-based phosphorescent Ir^{III} complexes **Ir-3Tz1F** and **Ir-3Tz2F**.

^{19}F NMR spectrum are consistent with the fluoro-substitution pattern of its ligand as well.

Thermal and photophysical properties

The thermal properties of the thiazole-based phosphorescent Ir^{III} complexes were characterized by both thermogravimetric analysis (TGA) and differential scanning calorimetry (DSC) under a nitrogen flow. The TGA results show that an evident decomposition process occurs at *ca.* 380 °C for **Ir-3Tz1F** and 365 °C for **Ir-3Tz2F** (Table 1 and Fig. S1a in the ESI†), which are much higher than their heteroleptic counterparts.[25] However, it seems that a slight decomposition of **Ir-3Tz2F** begins at *ca.* 160 °C (Fig. S1a, ESI†), indicating its poorer stability with respect to that of **Ir-3Tz1F**. This might be ascribed to the higher molecular activity of **Ir-3Tz2F** induced by the multiple highly polar C–F bonds.[37] The DSC traces for the homoleptic thiazole-based Ir^{III} complexes indicate high glass-transition temperatures (T_g) of *ca.* 215 °C for **Ir-3Tz1F** (Table 1 and Fig. S1b, ESI†). However, it appears that **Ir-3Tz2F** exhibits one exothermic process at *ca.* 165 °C and an endothermic process at *ca.* 220 °C (Fig. S1b, ESI†). With respect to the TGA curve for **Ir-3Tz2F** (Fig. S1a, ESI†), the former exothermic process should be induced by the slight decomposition of **Ir-3Tz2F**. Similar to that of **Ir-3Tz1F**, the glass-transition event occurring at *ca.* 220 °C for **Ir-3Tz2F** can be related to the distortion of the entire rigid molecular skeleton.

Both of the homoleptic thiazole-based Ir^{III} complexes show two distinct absorption bands in their UV-Vis spectra (Fig. 1 and Table 1). The high-energy strong UV absorption bands before 310 nm should be induced by the spin-allowed $S_1 \leftarrow S_0$ transitions of the organic ligands. On the contrary, the weaker and low-energy absorption located beyond 310 nm can be assigned to the charge transfer (CT) transitions in both singlet and triplet states. Clearly, the energy levels for the CT absorption bands fall in the order of **Ir-3Tz1F** < **Ir-3Tz2F** (Fig. 1).

Upon UV light irradiation at 360 nm, both the homoleptic thiazole-based Ir^{III} complexes emit strong phosphorescence in CH_2Cl_2 (Fig. 1 and Table 1). Their photoluminescence (PL) spectra display a double-peak pattern (Fig. 1). Clearly, the high-energy phosphorescent emission bands (*ca.* 529 nm for **Ir-3Tz1F** and 507 nm for **Ir-3Tz2F**) exhibit an unstructured line shape, whereas the low-energy ones (*ca.* 555 nm for **Ir-3Tz1F** and 533 nm for **Ir-3Tz2F**) show a well-structured line shape (Fig. 1 and Table 1). The triplet/phosphorescent character of these emission bands was supported by the long lifetime in the order of microseconds for the associated excited states.

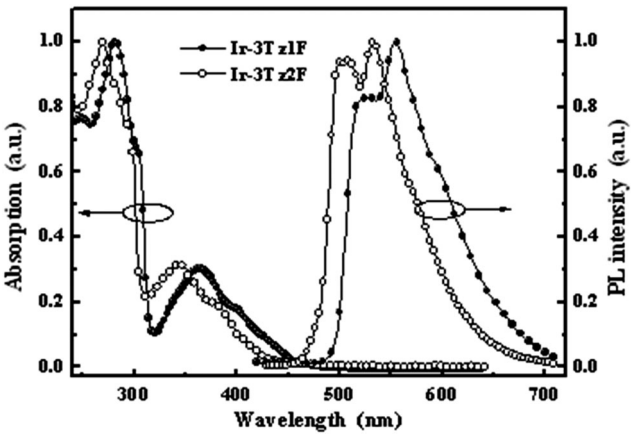

Fig. 1 UV-vis and photoluminescence (PL) spectra for the homoleptic thiazole-based phosphorescent Ir^{III} complexes.

In order to interpret the aforementioned photophysical results of these homoleptic thiazole-based phosphorescent Ir^{III} complexes, DFT calculations were carried out and the results are shown in Fig. 2 and Table 2. The DFT calculation results indicate that the lowest-energy transitions correspond to HOMO → LUMO (H → L) transitions with non-zero oscillator strengths for the S_1 states of the two homoleptic thiazole-based Ir^{III} complexes. However, the transitions HOMO → LUMO (H → L), HOMO → LUMO+1 (H → L+1), HOMO−2 → LUMO (H−2 → L) and HOMO−2 → LUMO+1 (H−2 → L+1) represent features of their T_1 states (Table 2), which are responsible for the phosphorescence in the two homoleptic thiazole-based Ir^{III} complexes. As indicated by the noticeably different contribution to the HOMO/HOMO−2 and LUMO/LUMO+1 from the metal d_π orbitals (Table 2 and Fig. 2), the lowest-energy excited states, S_1 and T_1, show evident metal-to-ligand charge transfer (MLCT) features. In addition, the intra-ligand charge transfer (ILCT) features from the phenyl ring to the thiazole unit can also be seen according to the distribution patterns of the critical transitions corresponding to the characters of the lowest-energy excited states S_1 and T_1 (Fig. 2). Hence, it can be concluded that the S_1 and T_1 states associated with the two homoleptic thiazole-based Ir^{III} complexes should consist of mixed MLCT and ILCT states. Therefore, the weak CT absorption bands in the UV-Vis spectra of **Ir-3Tz1F** and **Ir-3Tz2F** are induced by singlet and triplet MLCT states (^{1}MLCT and ^{3}MLCT) as well as those of ILCT states (^{1}ILCT and ^{3}ILCT).

Owing to the large contribution from the metal d_π orbitals to both the HOMO and HOMO−2 of the homoleptic thiazole-based

Table 1 Photophysical and thermostability data for the homoleptic thiazole-based Ir^{III} complexes

Complexes	Absorption λ_{abs}[a] (nm) 298 K	Emission λ_{em}[b] (nm) 298 K	Φ_P[c]	τ_P[d] (μs)	T_d/T_g (°C)
Ir-3Tz1F	249 (4.67), 281 (4.67), 303 (4.57), 364 (4.14), 402 (3.92), 434 (3.83)	525, 555	0.29	0.73 (525 nm), 1.61 (555 nm)	380/215
Ir-3Tz2F	270 (4.71), 283 (4.66), 295 (4.59), 343 (4.20), 382 (4.01), 418 (3.51)	508, 533	0.28	1.20 (507 nm), 1.33 (533 nm)	365/220

[a] Measured in CH_2Cl_2 at a concentration of 10^{-5} M, with log ε values shown in parentheses. [b] Measured in CH_2Cl_2 at a concentration of 10^{-5} M. [c] In degassed CH_2Cl_2 relative to *fac*-[Ir(ppy)$_3$] (Φ_P = 0.40), λ_{ex} = 360 nm. [d] Measured in degassed CH_2Cl_2 solutions at a sample concentration of *ca.* 10^{-5} M; the excitation wavelength was set at 355 nm for all the samples at 298 K.

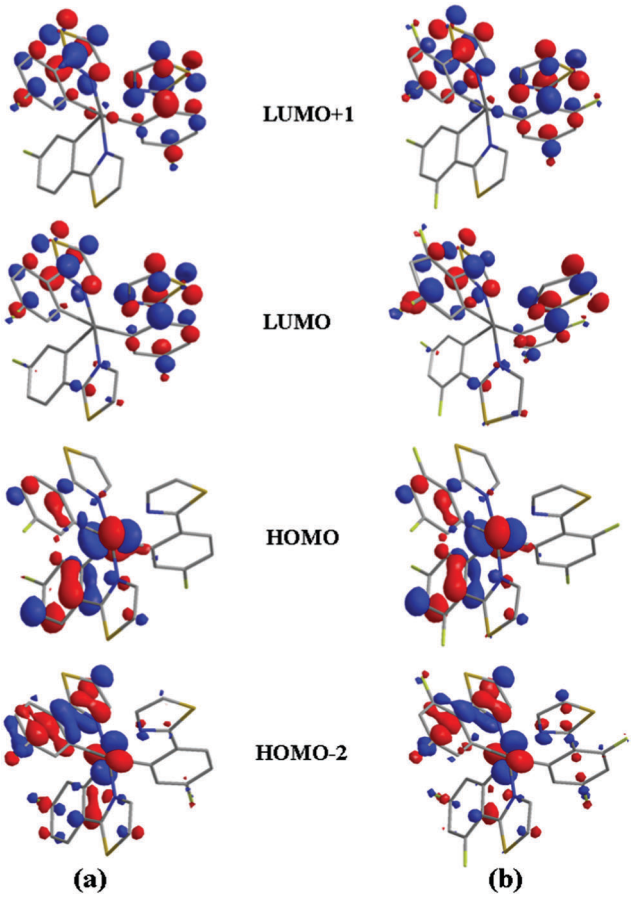

Fig. 2 Key frontier molecular orbitals corresponding to the important transition processes in (a) **Ir-3Tz1F** and (b) **Ir-3Tz2F**.

Ir^{III} complexes (Fig. 2 and Table 2), the molecular orbitals (MO) of the organic ligands and the metal center are mixed effectively to induce strong spin–orbit coupling effects. Therefore, triplet absorption bands occur with the feature of both ^{3}MLCT and ^{3}ILCT and induce the phosphorescent emission at 298 K (Fig. 1). According to the established relationship between the T_1 character and line shape of the phosphorescent spectra for the Ir^{III} complexes,[3,4] the high-energy broad and featureless phosphorescent band of the homoleptic thiazole-based Ir^{III} complexes can be assigned to the radiative decay of the ^{3}MLCT states, whereas the low-energy sharp phosphorescent band should come from the emissive decay of the ligand-centered ^{3}ILCT states (Fig. 1) due to its vibronic fine structure observed at a low temperature of 77 K (Fig. S1c, ESI†). Owing to the close energy levels for the ^{3}MLCT and ^{3}ILCT states (Fig. 1), there should be a competition between their radiative decay processes. Therefore, **Ir-3Tz1F** and **Ir-3Tz2F** exhibit dual emission bands (Fig. 1), as typically observed in ppy-type Ir^{III} phosphorescent complexes.[3,4] Similar to those of their analogues in the literature,[23,24] HOMO and HOMO−2 for both **Ir-3Tz1F** and **Ir-3Tz2F** are mainly located on the d_π orbitals of the Ir^{III} center and on the π orbitals of the phenyl rings. Hence, introducing a strongly electron-withdrawing –F group to the phenyl ring will stabilize the HOMO and HOMO−2 and lower their energy levels, which should increase the energy associated with the transitions corresponding to the T_1 states and elevate their energy levels. Hence, **Ir-3Tz1F** should possess T_1 states with lower energy levels to induce phosphorescence with a longer wavelength with respect to that of **Ir-3Tz2F**, which was shown by the PL spectra of the homoleptic thiazole-based Ir^{III} complexes (Fig. 1 and Table 1). Hence, there is good consistency between the experimental results and the theoretical calculations.

Electrochemical characterization

The electrochemical properties of the two homoleptic thiazole-based Ir^{III} complexes were investigated by cyclic voltammetry (CV) calibrated with ferrocene as the internal standard under a

Table 2 Contribution of the metal d_π orbitals to the key frontier molecular orbitals together with the TD-DFT calculation results

Compound	Contribution of metal d_π orbitals[a]	Contribution of metal d_π orbitals[a]	Largest coefficient in the CI expansion of the T_1 state ($S_0 \rightarrow T_1$ excitation energy)[b]	Largest coefficient in the CI expansion of the S_1 state ($S_0 \rightarrow S_1$ excitation energy)[b]	Oscillator strength (f) of the $S_0 \rightarrow S_1$ transition
Ir-3Tz1F	HOMO−2: 21.3% HOMO: 37.1%	LUMO+1: 3.4% LUMO: 1.5%	H → L: 0.34777 24.2% H → L+1: 0.22311 10.0% H−2 → L: 0.25445 12.9% H−2 → L+1: 0.25584 13.1% (489 nm)	H → L: 0.67760 91.8% H → L+1: 0.15807 5.0% (402 nm)	0.0407
Ir-3Tz2F	HOMO−2: 23.9% HOMO: 38.1%	LUMO+1: 3.6% LUMO: 1.6%	H → L: 0.30468 18.6% H → L+1: −0.21271 9.05% H−2 → L: 0.30397 18.5% H−2 → L+1: −0.27530 15.2% (470 nm)	H → L: 0.66742 89.1% H → L+1: −0.18832, 7.1% (381 nm)	0.0420

[a] Data were obtained by exporting DFT results with the software AOMix. [b] H → L represents the HOMO to LUMO transition. CI stands for configuration interaction.

Table 3 Redox properties of the thiazole-based Ir^{III} ppy-type complexes

Compound	E_a (V)	E_c (V)	HOMO[c] (eV)	LUMO[d] (eV)
Ir-3Tz1F	0.61[a]	−2.56[b]	−5.41	−3.01
Ir-3Tz2F	0.72[a]	−2.14[b]	−5.52	−3.43

[a] Reversible; the value was set as $E_{1/2}$. [b] Irreversible; the value was derived from the cathodic peak potential. [c] HOMO levels were calculated according to the equation HOMO = −(4.8 + E_a). [d] LUMO levels were obtained from the optical gap E_g.

nitrogen atmosphere. Both of the complexes showed a reversible oxidation couple (E_a) at *ca.* 0.61 V for **Ir-3Tz1F** and 0.72 V for **Ir-3Tz2F** (Table 3). With two –F groups on the phenyl ring of the ligand, the oxidation potential of **Ir-3Tz2F** moves markedly to a more positive region due to the stabilization effect on the HOMOs induced by the –F groups (*vide infra*). The reduction potentials (E_c) for the two complexes are located at *ca.* −2.56 V for **Ir-3Tz1F** and −2.14 V for **Ir-3Tz2F** (Table 3). From the MO patterns of the thiazole-based Ir^{III} complexes, it could be seen clearly that the phenyl rings of the organic ligands also make a large contribution to their LUMOs (Fig. 2). As a result, introducing more –F groups with a strong electron-withdrawing ability to the phenyl rings of the organic ligands should lower the LUMO levels of the thiazole-based Ir^{III} complexes and make them easier to be reduced. Therefore, **Ir-3Tz2F** possesses E_c at a less negative potential region with respect to **Ir-3Tz1F** (Table 3). The irreversibility of the reduction process of the complexes can be ascribed to their character being more susceptible to other environmental factors. The irreversible reduction processes of the two complexes during the cathodic sweep make their LUMO levels poorly reliable, as seen based on electrochemistry measurements. Therefore, we calculated their LUMO levels from the optical gap (E_g).

Electrophosphorescent characterization

The electrophosphorescent properties of **Ir-3Tz1F** and **Ir-3Tz2F** were characterized by phosphorescent OLEDs (PhOLEDs) with the configuration of ITO/MoO_3 (4 nm)/**CBP** (35 nm)/Ir x wt%:**CBP** (15 nm)/**TPBi** (40 nm)/LiF : Al (1 : 100 nm). Fig. 3 depicts the structures for both the multi-layer OLEDs made by vacuum deposition and the chemicals involved in the fabrication of the devices. In order to reduce the interfaces in the device and to benefit the EL performances, a doped 4,4′-*N*,*N*′-dicarbazolebiphenyl (**CBP**) layer served as both a hole-transporting layer and an emission layer. In order to optimize the EL efficiencies, doping-level dependent experiments were also carried out in the range from 6 to 10 wt%.

After applying the proper voltage, all the devices emit intense electrophosphorescence with the maxima at *ca.* 520 and 552 nm

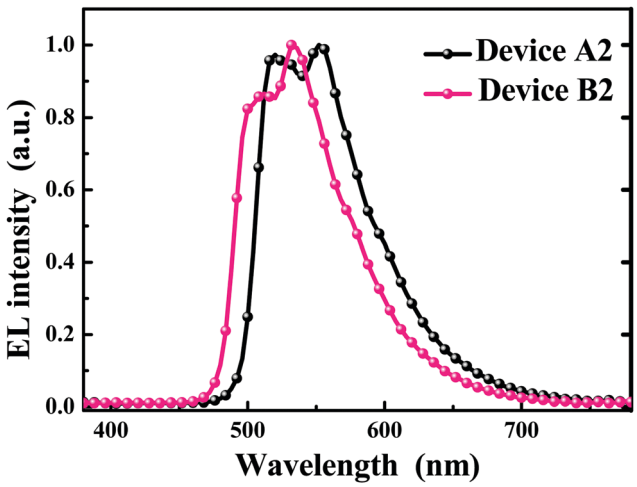

Fig. 4 EL spectra for the optimized devices **A2** and **B2** at *ca.* 8 V.

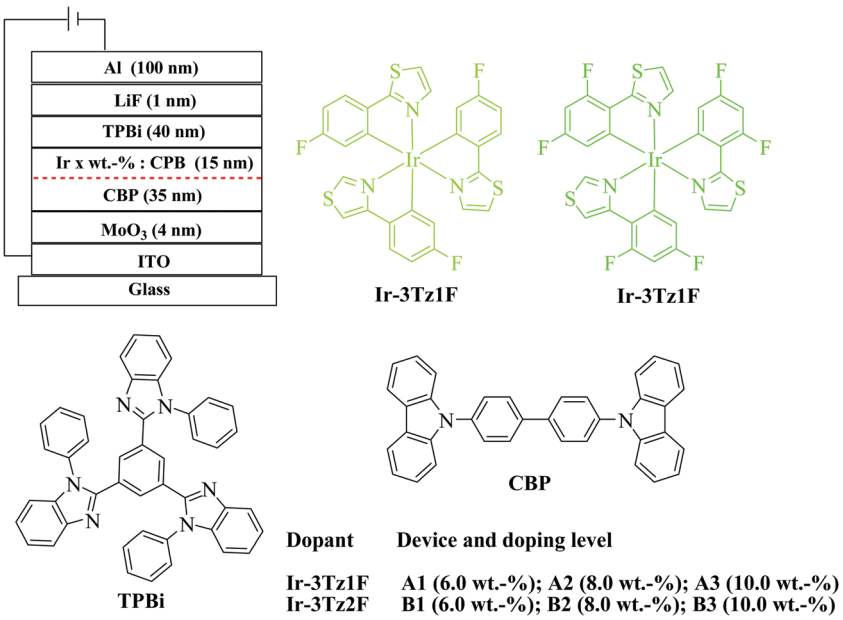

Fig. 3 General configuration of PhOLEDs made from **Ir-3Tz1F** and **Ir-3Tz2F** together with the molecular structures of the relevant compounds used in these devices.

Table 4 EL performance for all the PhOLEDs based on the homoleptic thiazole-based Ir^{III} complexes

Device	Phosphorescent dopant	$V_{turn\text{-}on}$ (V)	Luminance L (cd m^{-2})	η_{ext} (%)	η_L (cd A^{-1})	η_p (lm W^{-1})	λ_{max}[d] (nm)
A1	**Ir-3Tz1F** (6 wt%)	3.0	21 756 (9.5)[a]	14.1 (3.7)[a]	49.8 (3.8)	44.9 (3.2)	520, 552 (0.37, 0.58)
				14.0[b]	49.5	42.0	
				13.5[c]	47.0	35.0	
A2	**Ir-3Tz1F** (8 wt%)	3.0	25 957 (8.3)	15.8 (3.5)	56.2 (3.5)	50.2 (3.5)	520, 552 (0.37, 0.59)
				15.2	55.8	49.8	
				15.0	53.5	42.1	
A3	**Ir-3Tz1F** (10 wt%)	2.7	22 496 (8.9)	13.0 (3.5)	45.7 (3.5)	40.8 (3.5)	520, 552 (0.36, 0.58)
				12.7	45.0	38.1	
				12.0	42.1	31.1	
B1	**Ir-3Tz2F** (6 wt%)	3.1	24 803 (10.5)	6.1 (5.4)	20.1 (5.4)	13.8 (3.8)	512, 532 (0.32, 0.56)
				5.4	17.5	13.1	
				5.0	19.6	12.2	
B2	**Ir-3Tz2F** (8 wt%)	3.2	27 605 (9.5)	8.0 (4.8)	26.7 (4.6)	20.1 (3.5)	512, 532 (0.31, 0.58)
				7.1	21.6	19.6	
				7.9	26.5	18.7	
B3	**Ir-3Tz2F** (10 wt%)	3.3	26 760 (10.0)	7.4 (5.4)	24.6 (5.4)	17.1 (3.5)	512, 532 (0.32, 0.58)
				6.2	20.5	15.0	
				7.2	24.0	16.0	

[a] Maximum values of the devices. Values in parentheses are the voltages at which they were obtained. [b] Values collected at 100 cd m^{-2}. [c] Values collected at 1000 cd m^{-2}. [d] Values were collected at 8 V. CIE coordinates (x, y) are shown in parentheses.

for devices **A1–A3** and *ca.* 512 and 532 nm for devices **B1–B3** (Fig. 4, Table 4 and Fig. S2, ESI†). The current density (J)–voltage (V)–luminance (L) curves for the concerned devices are shown in Fig. 5 and Fig. S3 in the ESI,† and the relationship between the EL efficiencies and the current density for the devices are presented in Fig. 6 and Fig. S4 (ESI†). From Table 4, it can be clearly seen that device **A2** with an 8 wt% doping level of **Ir-3Tz1F** shows the best EL ability. The device **A2** doped with **Ir-3Tz1F** exhibits impressive EL performances with a low turn-on voltage of 3.0 V, a maximum luminance (L_{max}) of 25 957 cd m^{-2} at 8.3 V, a peak external quantum efficiency (η_{ext}) of 15.8%, a luminance efficiency (η_L) of 56.2 cd A^{-1} and a power efficiency (η_p) of 50.2 lm W^{-1} (Table 4 and Fig. 5, 6). Among the devices doped with **Ir-3Tz2F**, the device **B2** showed the best EL properties. It could be turned on at *ca.* 3.2 V and its light output could reach 27 605 cd m^{-2} at 9.4 V with peak EL efficiencies of 8.0%, 26.7 cd A^{-1} and 20.1 lm W^{-1} (Table 4 and Fig. 5, 6). Clearly, the EL capacity of **Ir-3Tz1F** was higher than that of **Ir-3Tz2F** (Table 4 and Fig. 6). This result can be ascribed to the following reasons: (1) The triplet

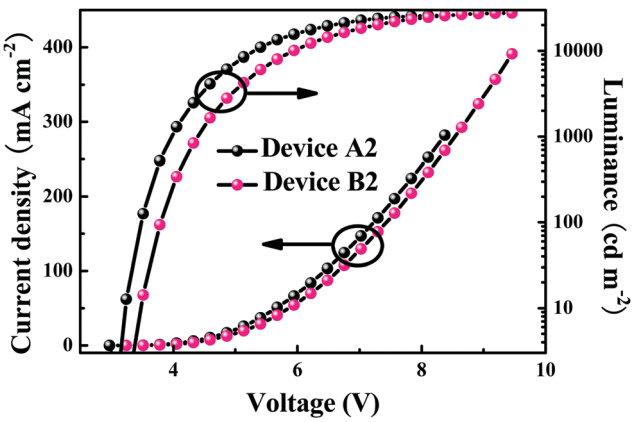

Fig. 5 Current density (J)–voltage (V)–luminance (L) curves for the optimized devices **A2** and **B2**.

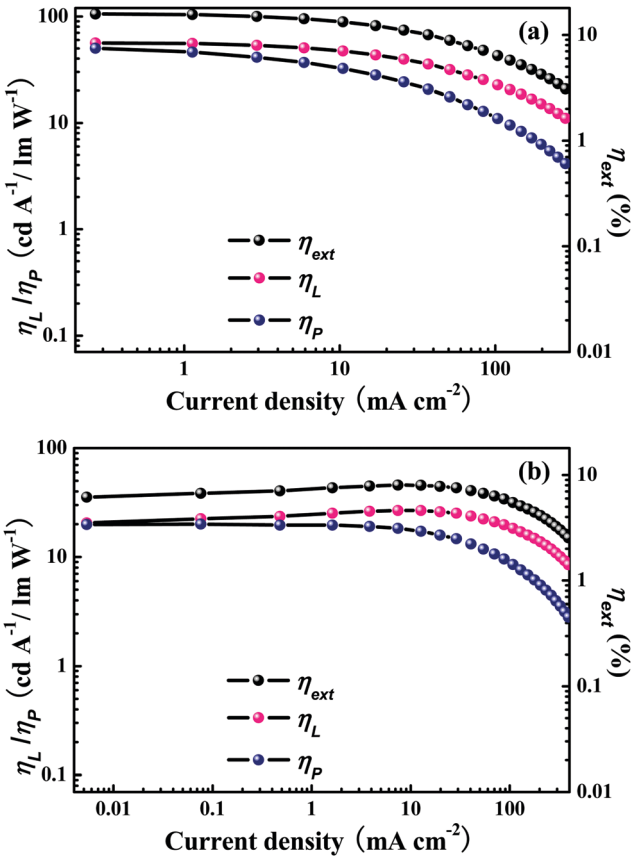

Fig. 6 Relationship between EL efficiencies and current density for the optimized devices (a) **A2** and (b) **B2**.

energy level (E_t) of **Ir-3Tz2F** is *ca.* 2.45 eV, which is quite close to that of the **CBP** host (*ca.* 2.62 eV). The small difference between their triplet energy levels should effectively enhance the possibility of an endothermic back energy transfer from the emissive triplet states of **Ir-3Tz2F** to the nonemissive triplet states of the **CBP** host.

Clearly, the undesired back energy transfer process would adversely affect the EL performance of **Ir-3Tz2F**. (2) According to the TGA results (Fig. S1, ESI†), **Ir-3Tz2F** is inclined to show a slight decomposition at lower temperature. Contamination in the emission layer of the device doped with **Ir-3Tz2F** will lower its EL efficiencies. Hence, **Ir-3Tz1F** exhibits a much better EL performance than that of **Ir-3Tz2F**.

From the aforementioned EL results of the monochromic PhOLEDs, the optimized devices can be turned on at low voltages of *ca.* 3.0 V (Table 4). Even at a high luminance of 1000 cd m^{-2}, the optimized device **A2** can still furnish decent EL efficiencies of 13.5%, 53.5 cd A^{-1} and 42.1 lm W^{-1} (Table 4 and Fig. 6). Recently, heteroleptic thiazole-based Ir^{III} analogues have been developed to show maximum EL efficiencies of 23.62 cd A^{-1}, 7.87% and 13.46 lm W^{-1} with the **CBP** host in PhOLEDs fabricated by vacuum deposition.[25] Functionalized thiazole-based Ir^{III} phosphorescent emitters with a TPA group have furnished attractive EL efficiencies of 39.97 cd A^{-1}, 14.82% and 34.95 lm W^{-1}.[24] In addition, high EL efficiencies of 30.84 cd A^{-1}, 12.88% and 26.17 lm W^{-1} have been achieved by Ir^{III} complexes bearing the 2-phenylthiazole-type ligand. Heteroleptic thiazole-based Ir^{III} phosphorescent emitters with picolinic acid derivatives as ancillary ligands can bring EL efficiencies of 10.98 cd A^{-1}, 6.08% and 6.89 lm W^{-1} in solution-processed OLEDs.[26] Compared with the aforementioned high EL performances achieved by thiazole-based Ir^{III} phosphorescent emitters, the great potential of these two homoleptic complexes in achieving high device efficiencies can be clearly seen.

Both the PL and EL spectra (Fig. 1 and 4) of the two homoleptic thiazole-based Ir^{III} complexes display a double-peak pattern, which can furnish emission bands in different wavelength regions. So, these phosphorescent emitters should show advantage to fabricate WOLEDs. Furthermore, our previous WOLEDs with thiazole-based Ir^{III} phosphorescent emitters bearing a TPA functional group showed undesired voltage-dependent white EL spectra.[24] Hence, it is necessary to construct highly efficient WOLEDs with these phosphorescent emitters to show stable white EL spectra. Considering high EL efficiencies as one of the preferential parameters for WOLEDs, **Ir-3Tz1F** with the higher EL performances was chosen to fabricate WOLEDs using the

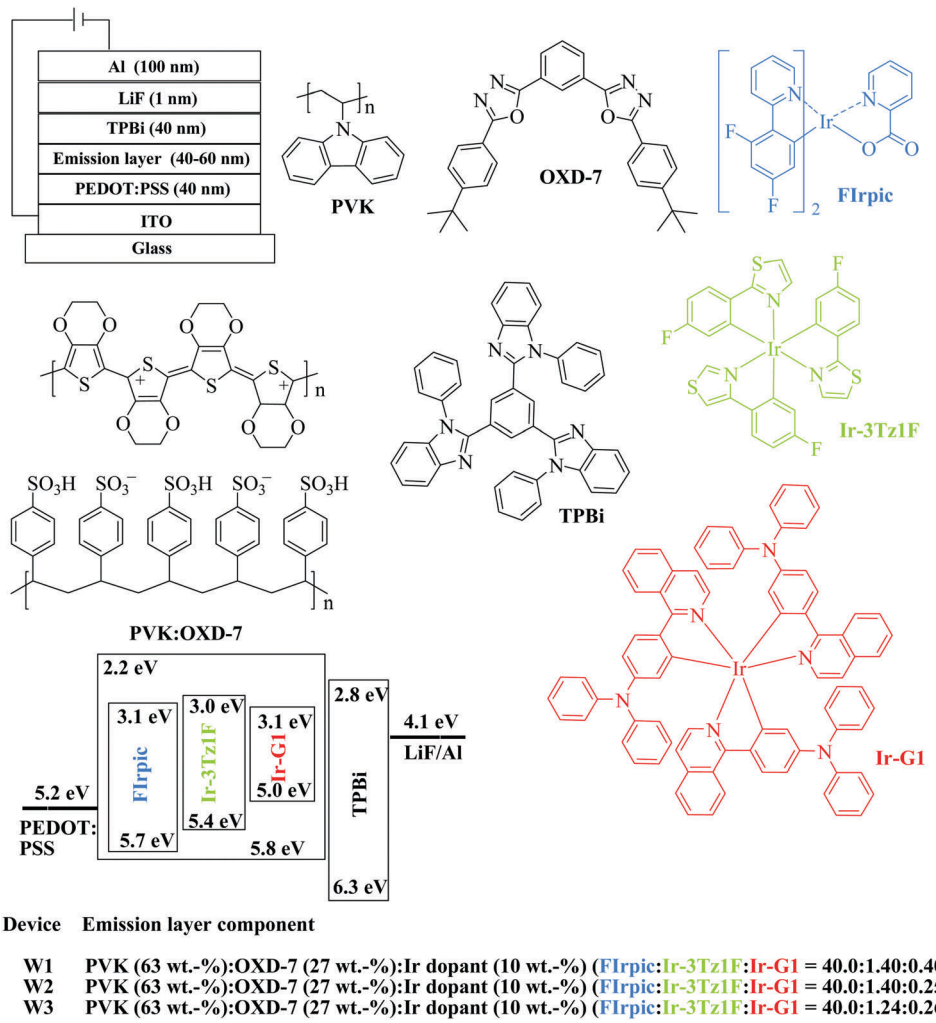

Fig. 7 Structure of the phosphorescent WOLEDs based on **Ir-3Tz1F** together with both the energy diagram and molecular structures of the relevant compounds used in these devices.

cheap and convenient solution-process technique. The configuration of the solution-processed WOLEDs is shown in Fig. 7. In addition to **Ir-3Tz1F**, the well-known blue phosphorescent **FIrpic** and the pure-red phosphorescent **Ir-G1** were employed to fulfill Red–Green–Blue (R–G–B) WOLEDs. All the three phosphorescent emitters were co-doped in **PVK** and **OXD-7** to form an emission layer by a simple spin-coating strategy. In order to optimize the EL performances, the ratio among the three phosphorescent emitters were tuned in the trichromatic WOLEDs.

For device **W1** with a weight ratio for **FIrpic** (Blue, B), **Ir-3Tz1F** (Green, G) and **Ir-G1** (Red, R) (B–G–R ratio) of 40 : 1.4 : 0.4, its EL spectra under a low driving voltage showed a red-emission dominated pattern (Fig. 8a). With increasing the driving voltage, the blue and green EL bands were enhanced to furnish a more balanced EL pattern (Fig. 8a). It is clear that both the EL spectra and the CIE coordinates of device **W1** are quite unstable with the variation in the driving voltage (Table 5 and Fig. 8a, 9). The voltage-dependent EL spectra in device **W1** can be explained as follows. From the energy-level diagram involved in these WOLEDs, it can be seen clearly that the red emitter **Ir-G1** possesses a high HOMO level due to the electron-rich TPA group used to furnish a strong hole-trapping ability (Fig. 7). Hence, the injected holes in the emission layer can be easily trapped by **Ir-G1**. At the same time, the LUMO level of **Ir-G1** is very close to that of **FIrpic** and **Ir-3Tz1F**. Therefore, the charge carriers injected in a small

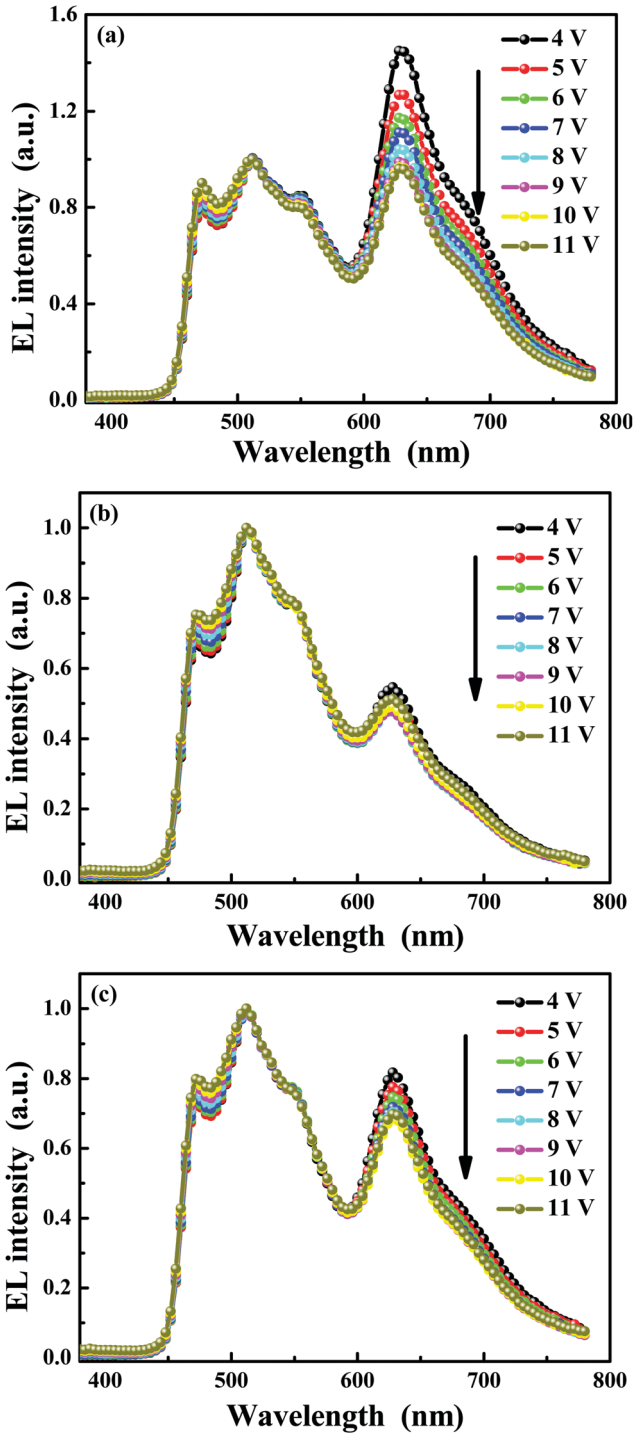

Fig. 8 EL spectra of the WOLEDs at different driving voltages. (a) **W1**, (b) **W2** and (c) **W3**.

Table 5 EL performance for all the solution-processed WOLEDs based on **Ir-3Tz1F**

		WOLEDs		
		W1	**W2**	**W3**
		B–G–R ratio = 40 : 1.4 : 0.4	B–G–R ratio = 40 : 1.4 : 0.25	B–G–R ratio = 40 : 1.24 : 0.26
$V_{turn\text{-}on}$ (V)		3.7	3.4	3.5
Luminance L^a (cd m^{-2})		9300	12 052	11 890
$\eta_{ext}{}^a$ (%)		16.4	14.8	16.5
$\eta_L{}^a$ (cd A^{-1})		31.3	34.6	33.4
$\eta_P{}^a$ (lm W^{-1})		25.5	31.8	30.6
CIE/CRI	4 V	(0.40, 0.43)/78	(0.33, 0.47)/70	(0.35, 0.45)/79
	5 V	(0.39, 0.43)/81	(0.33, 0.47)/68	(0.35, 0.45)/80
	6 V	(0.38, 0.43)/82	(0.32, 0.47)/66	(0.35, 0.45)/79
	7 V	(0.38, 0.44)/83	(0.32, 0.47)/67	(0.34, 0.45)/78
	8 V	(0.37, 0.44)/83	(0.32, 0.47)/67	(0.34, 0.45)/78
	9 V	(0.37, 0.43)/83	(0.32, 0.46)/67	(0.34, 0.45)/78
	10 V	(0.36, 0.43)/82	(0.32, 0.46)/68	(0.34, 0.45)/78
	11 V	(0.36, 0.43)/82	(0.32, 0.46)/69	(0.34, 0.44)/78

[a] Maximum values.

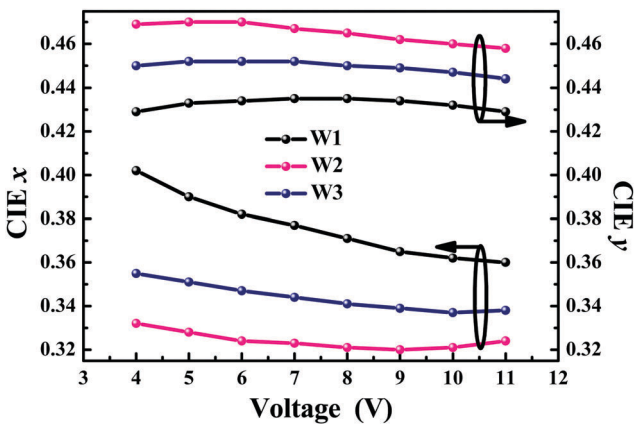

Fig. 9 Dependence of the CIE coordinates of the solution-processed WOLEDs on the driving voltages.

number at a low driving voltage can easily recombine on **Ir-G1** molecules to enhance the red EL band in the EL spectra. This situation will greatly reduce the chance of charge recombination on **FIrpic** and **Ir-3Tz1F** molecules and weaken the EL bands from **FIrpic** and **Ir-3Tz1F**. In addition, the inevitable cascade energy transfer processes from **FIrpic** to **Ir-3Tz1F** and then to **Ir-G1** enhance the red EL band. Hence, device **W1** exhibits red-emission dominated EL spectra at low driving voltages. However, with increasing the driving voltage, too many charge carriers are injected into the emission layer to be consumed by the **Ir-G1** molecules due to their low content in the emission layer. A lot of the remaining charge carriers can recombine on **FIrpic** and **Ir-3Tz1F** molecules to substantially enhance the blue and green EL bands (Fig. 8a), and the cascade energy transfer processes cannot effectively weaken the blue and green EL bands due to the low content of **Ir-G1**. Hence, device **W1** exhibits voltage-dependent EL spectra (Fig. 8a). From the discussion above, it is clear that the red emitter **Ir-G1** can play a critical role in inducing the undesired voltage-dependent EL spectra.

In order to weaken the effect of the red emitter **Ir-G1** in inducing unstable white EL spectra, the most feasible way is to reduce the content of the red emitter **Ir-G1** in the emission layer. Based on this idea, device **W2** with a B–G–R ratio of 40 : 1.4 : 0.25 in its emission layer was constructed. Encouragingly, both the EL spectra and the CIE coordinates of device **W2** can be maintained as very stable in a wide range of driving voltages (Fig. 8b, 9 and Table 5). The much lower content of **Ir-G1** in the emission layer of device **W2** will effectively eliminate its negative effect on the charge carrier recombination on **FIrpic** and **Ir-3Tz1F** molecules as well as on the cascade energy transfer processes. Accordingly, the EL spectra of device **W2** can be maintained as very stable in a wide range of driving voltages (Fig. 8b).

Typically, red emitters exhibit relatively lower EL efficiencies. Hence, compared with those of device **W1**, the EL efficiencies of device **W2** were improved due to the lower content of **Ir-G1** (Table 5 and Fig. S5, S6, ESI†). Device **W2** could furnish peak EL efficiencies of 34.6 cd A^{-1}, 14.8% and 31.8 lm W^{-1} (Fig. S5 and S6, ESI†), representing some of the most attractive EL performances ever achieved by solution-processed R–G–B WOLEDs. Despite the high EL efficiencies and stable white EL spectra, device **W2** displayed relatively unbalanced white EL spectra with a low red-light component. As a result, the white light emitted from device **W2** possessed a low color rendering index (CRI) of generally <70 (Table 5). Clearly, device **W2** showed green-dominated white EL spectra. Hence, one of the most feasible ways to achieve balanced white EL spectra is to reduce the content of **Ir-3Tz1F** in the emission layer. From the EL behaviors of both **W1** and **W2**, a higher content of **Ir-G1** can evidently increase the red-light component in the white light EL spectra and reduce the EL efficiencies at the same time. Therefore, a reasonable strategy for achieving the optimized trade-off among stable balanced white EL spectrum, high EL efficiency and high CRI is to reduce the content of **Ir-3Tz1F** in the emission layer as well as to slightly increase the **Ir-G1** content. Hence, device **W3** with a B–G–R ratio of 40 : 1.24 : 0.26 was fabricated. From the EL performances, it can be seen that device **W3** could achieve a maximum luminance of 11 890 cd m^{-2} (Fig. 10 and Table 5). Importantly, device **W3** showed much more

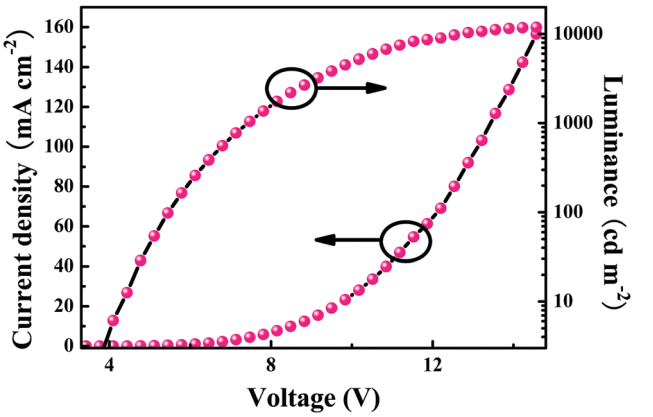

Fig. 10 Current density (*J*)–voltage (*V*)–luminance (*L*) curves for the optimized device **W3**.

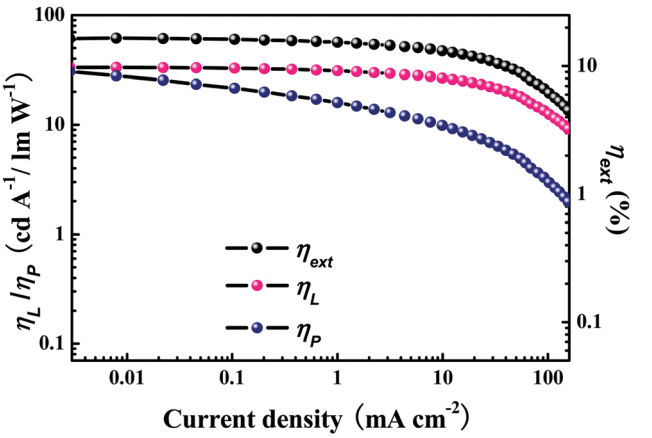

Fig. 11 Relationship between the EL efficiencies and the current density for the optimized device **W3**.

balanced stable white EL spectra with a CRI of about 80 than device **W2** while maintaining high EL efficiencies of 33.4 cd A^{-1}, 16.5% and 30.6 lm W^{-1} (Fig. 11 and Table 5), nearly identical to device **W2**. Hence, an excellent trade-off among stable balanced white EL spectrum, high EL efficiency and high CRI was successfully fulfilled in device **W3**. Thiazole-based Ir^{III} phosphorescent complexes have been rarely introduced into WOLEDs. In our previous work, we prepared orange phosphorescent thiazole-based Ir^{III} complexes with a TPA functional group to construct WOLEDs through both vacuum deposition and solution-processing strategies.[24] The highest EL efficiencies of the concerned WOLEDs were 22.72 cd A^{-1}, 9.06% and 17.28 lm W^{-1}. In addition, the white EL spectra of the devices exhibited serious voltage-dependent characters, with the highest CRI of *ca.* 72.[24] To the best of our knowledge, device **W3** represents the most state-of-the-art WOLED made from thiazole-based Ir^{III} phosphorescent emitters.

Conclusions

Two homoleptic thiazole-based cyclometalated Ir^{III} phosphorescent complexes were successfully developed. Their thermal stability,

photophysical properties, electrochemistry and EL performances were carefully investigated. Owing to their advanced photophysical and electrochemical features, the phosphorescent homoleptic thiazole-based Ir^{III} emitters exhibited high EL efficiencies in monochromic PhOLEDs with η_{ext} of 15.8%, η_L of 56.2 cd A^{-1} and η_p of 50.2 lm W^{-1}. Importantly, an excellent trade-off between stable a balanced white EL spectrum and a high EL efficiency was successfully realized in solution-processed trichromatic WOLEDs based on these homoleptic thiazole-based Ir^{III} phosphorescent emitters. The optimized solution-processed WOLED with three primary colors showed very attractive EL efficiencies of 33.4 cd A^{-1}, 16.5% and 30.6 lm W^{-1}, while maintaining both high a CRI of *ca.* 80 and very stable white EL spectra in a wide voltage range. All these decent results represent the top-ranking EL performances ever achieved by thiazole-based Ir^{III} phosphorescent emitters, indicating their great potential in the field of PhOLEDs.

Acknowledgements

This research was financially supported by the Fundamental Research Funds for the Central Universities (cxtd2015003), The Program for New Century Excellent Talents in University, the Ministry of Education of China (NECT-09-0651), the Key Creative Scientific Research Team in Shaanxi Province (2013KCT-05), the China Postdoctoral Science Foundation (Grant no. 20130201110034, 2014M562403), and the National Natural Science Foundation of China (no. 20902072, 21572176). The financial support from State Key Laboratory for Mechanical Behavior of Materials is also acknowledged. W.-Y. W. acknowledges the financial support from the National Basic Research Program of China (973 Program, grant no. 2013CB834702), the Areas of Excellence Scheme, University Grants Committee of HKSAR, China (AoE/P-03/08), Hong Kong Research Grants Council (HKBU 12304715), Hong Kong Baptist University (FRG1/14-15/084) and the Hong Kong Polytechnic University.

References

1 W.-Y. Wong, S.-M. Chan, K.-H. Choi, K.-W. Cheah and W.-K. Chan, *Macromol. Rapid Commun.*, 2000, **21**, 453.
2 X. Yang, G. Zhou and W. Y. Wong, *Chem. Soc. Rev.*, 2015, **44**, 8484.
3 S. Lamansky, P. Djurovich, D. Murphy, F. Abdel-Razzaq, H.-E. Lee, C. Adachi, P. E. Burrows, S. R. Forrest and M. E. Thompson, *J. Am. Chem. Soc.*, 2001, **123**, 4304.
4 A. Tsuboyama, H. Iwawaki, M. Furugori, T. Mukaide, J. Kamatani, S. Igawa, T. Moriyama, S. Miura, T. Takiguchi, S. Okada, M. Hoshino and K. Ueno, *J. Am. Chem. Soc.*, 2003, **125**, 12971.
5 Y. Chi and P. T. Chou, *Chem. Soc. Rev.*, 2010, **39**, 638.
6 Y. You and S. Y. Park, *Dalton Trans.*, 2009, 1267.
7 L. Xiao, Z. Chen, B. Qu, J. Luo, S. Kong, Q. Gong and J. Kido, *Adv. Mater.*, 2011, **23**, 926.
8 X. Yang, X. Xu, J. Zhao, J. Dang, Z. Huang, X. Yan, G. Zhou and D. Wang, *Inorg. Chem.*, 2014, **53**, 12986.
9 X. Xu, X. Yang, Y. Wu, G. Zhou, C. Wu and W.-Y. Wong, *Chem. – Asian J.*, 2015, **10**, 252.
10 C. Fan and C. Yang, *Chem. Soc. Rev.*, 2014, **43**, 6439.
11 Q. Wang, I. W. Oswald, X. Yang, G. Zhou, H. Jia, Q. Qiao, Y. Chen, J. Hoshikawa-Halbert and B. E. Gnade, *Adv. Mater.*, 2014, **26**, 8107.
12 C. W. Tang and S. A. Vanslyke, *Appl. Phys. Lett.*, 1987, **51**, 913.
13 J. Kido, M. Kimura and K. Nagai, *Science*, 1995, **267**, 1332.
14 J.-L. Liao, Y. Chi, Y.-D. Su, H.-X. Huang, C.-H. Chang, S.-H. Liu, G.-H. Lee and P.-T. Chou, *J. Mater. Chem. C*, 2014, **2**, 6269.
15 H. B. Wu, L. Ying, W. Yang and Y. Cao, *Chem. Soc. Rev.*, 2009, **38**, 3391.
16 J. Brooks, Y. Babayan, S. Lamansky, P. I. Djurovich, I. Tsyba, R. Bau and M. E. Thompson, *Inorg. Chem.*, 2002, **41**, 3055.
17 R. Wang, D. Liu, H. Ren, T. Zhang, H. Yin, G. Liu and J. Li, *Adv. Mater.*, 2011, **23**, 2823.
18 D. Liu, H. Ren, L. Deng and T. Zhang, *ACS Appl. Mater. Interfaces*, 2013, **5**, 4937.
19 R. Wang, D. Liu, H. Ren, T. Zhang, X. Wang and J. Li, *J. Mater. Chem.*, 2011, **21**, 15494.
20 R. Wang, L. Deng, T. Zhang and J. Li, *Dalton Trans.*, 2012, **41**, 6833.
21 J. Li, R. Wang, R. Yang, W. Zhou and X. Wang, *J. Mater. Chem. C*, 2013, **1**, 4171.
22 J. Dai, K. Zhou, M. Li, H. Sun, Y. Chen, S. Su, X. Pu, Y. Huang and Z. Lu, *Dalton Trans.*, 2013, **42**, 10559.
23 X. Xu, Y. Zhao, J. Dang, X. Yang, G. Zhou, D. Ma, L. Wang, W.-Y. Wong, Z. Wu and X. Zhao, *Eur. J. Inorg. Chem.*, 2012, 2278.
24 X. Yang, Y. Zhao, X. Zhang, R. Li, J. Dang, Y. Li, G. Zhou, Z. Wu, D. Ma, W.-Y. Wong, X. Zhao, A. Ren, L. Wang and X. Hou, *J. Mater. Chem.*, 2012, **22**, 7136.
25 C. Yao, B. Jiao, X. Yang, X. Xu, J. Dang, G. Zhou, Z. Wu, X. Lv, Y. Zeng and W.-Y. Wong, *Eur. J. Inorg. Chem.*, 2013, 4754.
26 T. Giridhar, W. Cho, J. Park, J.-S. Park, Y.-S. Gal, S. Kang, J. Y. Lee and S.-H. Jin, *J. Mater. Chem. C*, 2013, **1**, 2368.
27 Q. Wang, J. Ding, D. Ma, Y. Cheng, L. Wang, X. Jing and F. Wang, *Adv. Funct. Mater.*, 2009, **19**, 84.
28 X. Yang, G. Zhou and W.-Y. Wong, *J. Mater. Chem. C*, 2014, **2**, 1760.
29 K. A. King, P. J. Spellane and R.-J. Watts, *J. Am. Chem. Soc.*, 1985, **107**, 1431.
30 M. Thelakkat and H.-W. Schmidt, *Adv. Mater.*, 1998, **10**, 219.
31 G. J. Zhou, W. Y. Wong, B. Yao, Z. Y. Xie and L. X. Wang, *Angew. Chem., Int. Ed.*, 2007, **46**, 1149.
32 W. R. Wadt and P. J. Hay, *J. Chem. Phys.*, 1985, **82**, 284.
33 P. J. Hay and W. R. Wadt, *J. Chem. Phys.*, 1985, **82**, 299.
34 M. J. Frisch, G. W. Trucks, H. B. Schlegel, G. E. Scuseria, M. A. Robb, J. R. Cheeseman, J. A. Montgomery, T. Vreven Jr., K. N. Kudin, J. C. Burant, J. M. Millam, S. S. Iyengar, J. Tomasi, V. Barone, B. Mennucci, M. Cossi, G. Scalmani, N. Rega, G. A. Petersson, H. Nakatsuji, M. Hada, M. Ehara, K. Toyota, R. Fukuda, J. Hasegawa, M. Ishida, T. Nakajima, Y. Honda, O. Kitao, H. Nakai, M. Klene, X. Li, J. E. Knox,

H. P. Hratchian, J. B. Cross, V. Bakken, C. Adamo, J. Jaramillo, R. Gomperts, R. E. Stratmann, O. Yazyev, A. J. Austin, R. Cammi, C. Pomelli, J. W. Ochterski, P. Y. Ayala, K. Morokuma, G. A. Voth, P. Salvador, J. J. Dannenberg, V. G. Zakrzewski, S. Dapprich, A. D. Daniels, M. C. Strain, O. Farkas, D. K. Malick, A. D. Rabuck, K. Raghavachari, J. B. Foresman, J. V. Ortiz, Q. Cui, A. G. Baboul, S. Clifford, J. Cioslowski, B. B. Stefanov, G. Liu, A. Liashenko, P. Piskorz, I. Komaromi, R. L. Martin, D. J. Fox, T. Keith, M. A. Al-Laham, C. Y. Peng, A. Nanayakkara, M. Challacombe, P. M. W. Gill, B. Johnson, W. Chen, M. W. Wong, C. Gonzalez and J. A. Pople, *Gaussian 09, revision A.2*, Gaussian, Inc., Wallingford, CT, 2009.

35 R. Pis Diez, *MullPop*, The National University of La Plata, Argentina, 2003.

36 G. Schaftenaar, *Molden* v3.7, CAOS/CAMM Center Nijmegen, Toernooiveld, Nijmegen, The Netherlands, 2001.

37 J. Zhao, Y. Yu, X. Yang, X. Yan, H. Zhang, X. Xu, G. Zhou, Z. Wu, Y. Ren and W.-Y. Wong, *ACS Appl. Mater. Interfaces*, 2015, 7, 24703.